applied sciences

MDPI

Article

Improving the Fuel Economy and Battery Lifespan in Fuel Cell/Renewable Hybrid Power Systems Using the Power-Following Control of the Fueling Regulators

Nicu Bizon [1,2,*], Mihai Oproescu [1], Phatiphat Thounthong [3,4], Mihai Varlam [2], Elena Carcadea [2], Mihai Culcer [2], Mariana Iliescu [2], Maria Simona Raboaca [2] and Ioan Sorin Sorlei [2]

1 Faculty of Electronics, Communication and Computers, University of Pitesti, 110040 Pitesti, Romania; mihai.oproescu@upit.ro
2 ICSI Energy, National Research and Development Institute for Cryogenic and Isotopic Technologies, 240050 Ramnicu Valcea, Romania; mihai.varlam@icsi.ro (M.V.); elena.carcadea@icsi.ro (E.C.); mihai.culcer@icsi.ro (M.C.); mariana.iliescu@icsi.ro (M.I.); simona.raboaca@icsi.ro (M.S.R.); sorin.sorlei@icsi.ro (I.S.S.)
3 Renewable Energy Research Centre (RERC), King Mongkut's University of Technology North Bangkok, 1518, Pracharat 1 Road, Bangsue, Bangkok 10800, Thailand; phatiphat.t@fte.kmutnb.ac.th
4 Groupe de Recherche en Energie Electrique de Nancy (GREEN), Université de Lorraine, F-54000 Nancy, France
* Correspondence: nicu.bizon@upit.ro

Received: 1 November 2020; Accepted: 20 November 2020; Published: 23 November 2020

Abstract: In this study, the performance and safe operation of the fuel cell (FC) system and battery-based energy storage system (ESS) included in an FC/ESS/renewable hybrid power system (HPS) is fully analyzed under dynamic load and variable power from renewable sources. Power-following control (PFC) is used for either the air regulator or the fuel regulator of the FC system, or it is switched to the inputs of the air and hydrogen regulators based on a threshold of load demand; these strategies are referred to as air-PFC, fuel-PFC, and air/fuel-PFC, respectively. The performance and safe operation of the FC system and battery-based ESS under these strategies is compared to the static feed-forward (sFF) control used by most commercial strategies implemented in FC systems, FC/renewable HPSs, and FC vehicles. This study highlights the benefits of using a PFC-based strategy to establish FC-system fueling flows, in addition to an optimal control of the boost power converter to maximize fuel economy. For example, the fuel economy for a 6 kW FC system using the air/fuel-PFC strategy compared to the strategies air-PFC, fuel-PFC, and the sFF benchmark is 6.60%, 7.53%, and 12.60% of the total hydrogen consumed by these strategies under a load profile of up and down the stairs using 1 kW/2 s per step. For an FC/ESS/renewable system, the fuel economy of an air/fuel-PFC strategy compared to same strategies is 7.28%, 8.23%, and 13.43%, which is better by about 0.7% because an FC system operates at lower power due to the renewable energy available in this case study.

Keywords: fuel cell; hydrogen economy; fuel starvation; safe operation; electrical energy efficiency

1. Introduction

A report by the Intergovernmental Panel on Climate Change (IPCC) noted that so far the global temperature has risen by 1 °C due to warming by 0.2 °C per decade and may reach a critical value of 2 °C by the 2060s if the proposed environmental policies will not be implemented urgently worldwide [1].

This global warming has caused the warmest 18 years to date as well as several meteorological events that fall into the extreme intensity class, and for some time now it has been increasingly recognized and accepted that greenhouse gas (GHG) emissions are responsible for most of these climate changes [1,2].

As it is well known, the largest source of GHG emissions from human activities (formed mostly by carbon dioxide, accounting for 80% of the emissions) is represented by the energy-producing industry and by transportation, both of which are responsible together for more than a half of the total emission [3]. Given this situation, it becomes obvious there is the need to increase research and technology development efforts to make the transition to a low-carbon, secure, and competitive economy [4].

Part of this problem solution is perceived to be the increase in using renewable energy sources (RESs) [5]. Unfortunately, the rapid deployment of RESs involves addressing issues related to their disadvantages because there are some [6].

Their vast majority is characterized by intermittency and fairly wide diurnal and/or seasonal variability [7]. Due to their inherent nature, RESs are vulnerable to climate change and are also geographically unevenly distributed, and so the redistribution of energy, with all the losses involved, becomes inevitable [8].

During the last few years, technology advances have progressed in establishing a carbon-free energy chain via a partnership between electricity and hydrogen, mediated by fuel cells, which act as efficient and pollution-free energy converters, allowing direct conversion of hydrogen to electricity and thus favoring RES growing scale applicability [9]. To this effect, the proton exchange membrane fuel cell (PEMFC) emerged as a candidate solution [10], due to the advantages such as the high efficiency, zero emission, low noise, and flexibility in controllable power output. In addition, if we refer to PEMFC performance, then it should be mentioned that it strongly depends on operating parameters (such as load profile, temperature, pressure, relative humidity, reactance stoichiometry, etc.) that can cause significant changes in PEMFC performance [11].

Nevertheless, the slowness in some of the balance of plant auxiliary subsystems for gas (fuel and oxidizer), heat, and water management operation, and also in electrochemical processes occurring in fuel cells themselves, makes an FC-based energy storage or power supply system unable to provide a quick startup and to follow fast load changes [12].

It is a fact that in real life, electricity consumption characteristics are hilly and, moreover, quite often fast transients occur, so it appears obvious there is the need to use in power systems, apart from fuel cells, some wide dynamics energy storage devices to help the power source match the load demand [13]. Together, they form a so-called hybrid power system (HPS).

Usually, hybridization is made using batteries and/or ultracapacitors (UCs) [14]. As it is known, a lithium-ion battery has a high energy ratio, a relatively long life compared to other technologies for making batteries, and can generate high power [15], and an ultracapacitor has high power density and very short response time [16]; together or separately, they can counterbalance the disadvantages of pure FC power systems [17].

Regardless of the application that a HPS works in, be it mobile or stationary, the power distribution among FCs, batteries, and/or ultracapacitors is a basic problem to be solved through an energy management strategy (EMS) [18]. Moreover, in the car propulsion system, these storage devices allow for the absorption of braking energy, thus improving efficiency and also eliminating the requirement for a starting device [19].

The way in which the HPS control strategy is designed has a decisive influence both on its performance [20] and on the economic aspects [21]. System performance control aims to optimize the static and dynamic characteristics and also to maintain a low current fluctuation of FCs [21,22] and a narrow range of charging and discharging depth of the energy storage devices, in order to preserve their lifespan [14,17,19,23]. System economics control often involves improving economic efficiency

through several means, such as reducing the fuel [24] and/or energy consumption [25] and maximizing energy efficiency [26].

An EMS aims at finding an optimal solution [27] for the specific system by considering several or all the mentioned aspects [19,20,28–30]. Especially in the last decade, more attention has been paid to different topologies of multisource hybrid electric power systems used in mobility energy supply [31] and in stationary and portable power generation [32]. The major challenges faced by the ongoing research involve the integration of multiple and often conflicting objectives of power management strategy optimization in a real-time control system [33]. The EMS of a fuel cell hybrid power systems should aim at improving the system design (topology, dimensions, weight etc.), performances (fuel consumption, energy efficiency, lifespan, resilience, etc.) and cost, and at finding an optimal solution for the specific system by considering aforementioned objectives.

The main objective of this paper is to carry out a systematic evaluation of four fuel economy EMSs, three of which involves power-following control (PFC). These EMSs are referred to as air/fuel-PFC, air-PFC, fuel-PFC, and static feed-forward (sFF) strategies, and they are assessed in order to identify the best and safest strategy compared to the commercial standard based on the static feed-forward (sFF) control. For this, indicators such as fuel economy and oxygen excess ratio (OER) are used to evaluate the efficient and safe operation of an FC system and battery using power-following control (PFC) for the air regulator or the fuel regulator of the FC system, either separately or switched. The innovative switched mode proposed for the air/fuel-PFC strategy is comparatively analyzed with PFC-based strategies that control separately the air regulator or the fuel regulator of the FC system in order to highlight the fuel economy obtained for FC systems and FC/renewable hybrid power systems (HPSs). Net FC power is generated by PFC-based strategies for battery operation in sustained charging mode, with increased battery lifespan and cost less maintenance of the HPS.

Following this objective, the structure of the paper is as follows. The first section details the model of an FC/renewable HPS, a PFC-based fuel economy EMS, and the involved control and optimization loops. The second section presents and comments on the results obtained under dynamic load and variable power from renewable energy sources (RESs). The last two sections discuss the results and conclude the paper respectively.

2. Materials and Methods

The fuel cell (FC) system, battery/ultracapacitor (UC) hybrid ESS, and FC/ESS/renewable hybrid power system (HPS) represented in Figure 1 are analyzed under dynamic load and variable power from renewable energy sources (RESs) respectively, with the preliminary results under dynamic load presented in [34]. The load profile that was chosen was up and down the stairs with levels changed at every 2 ms using a step of 1 kW (see P_{Load} at the top of Figure 2). The renewable energy profile (see P_{RES} in the 2nd plot of Figure 2) was generated by adding the power from two renewable sources, such as the power generated by a photovoltaic park and a wind turbine farm (see P_{RES1} and P_{RES2} in the 3rd plot of Figure 2), and the random profile with 1 kW peak (P_{RES3} in the 4th plot of Figure 2):

$$P_{RES} = P_{RES1} + P_{RES2} + P_{RES3} \quad (1)$$

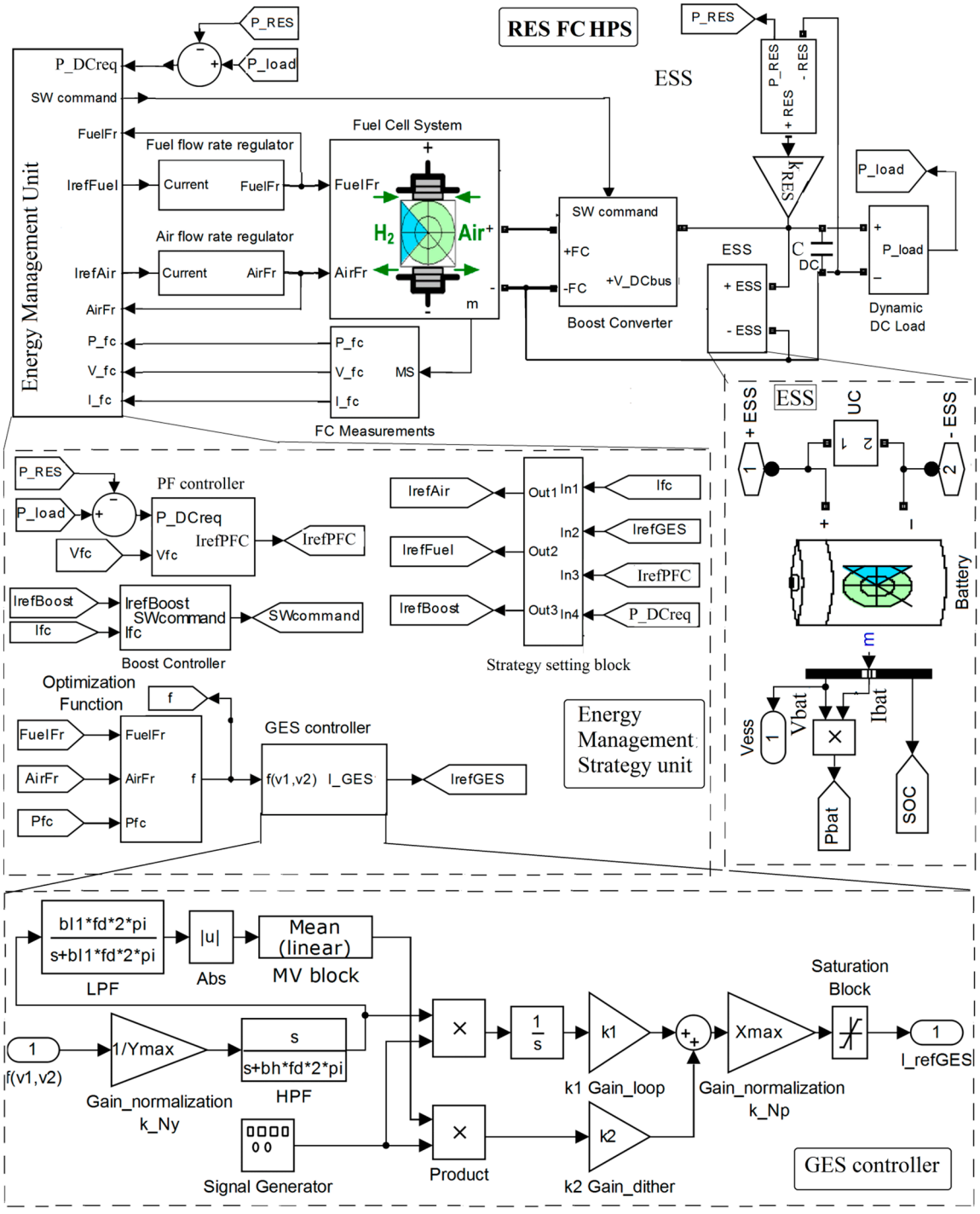

Figure 1. Fuel cell/energy storage system (FC/ESS) renewable hybrid power system (HPS) [34].

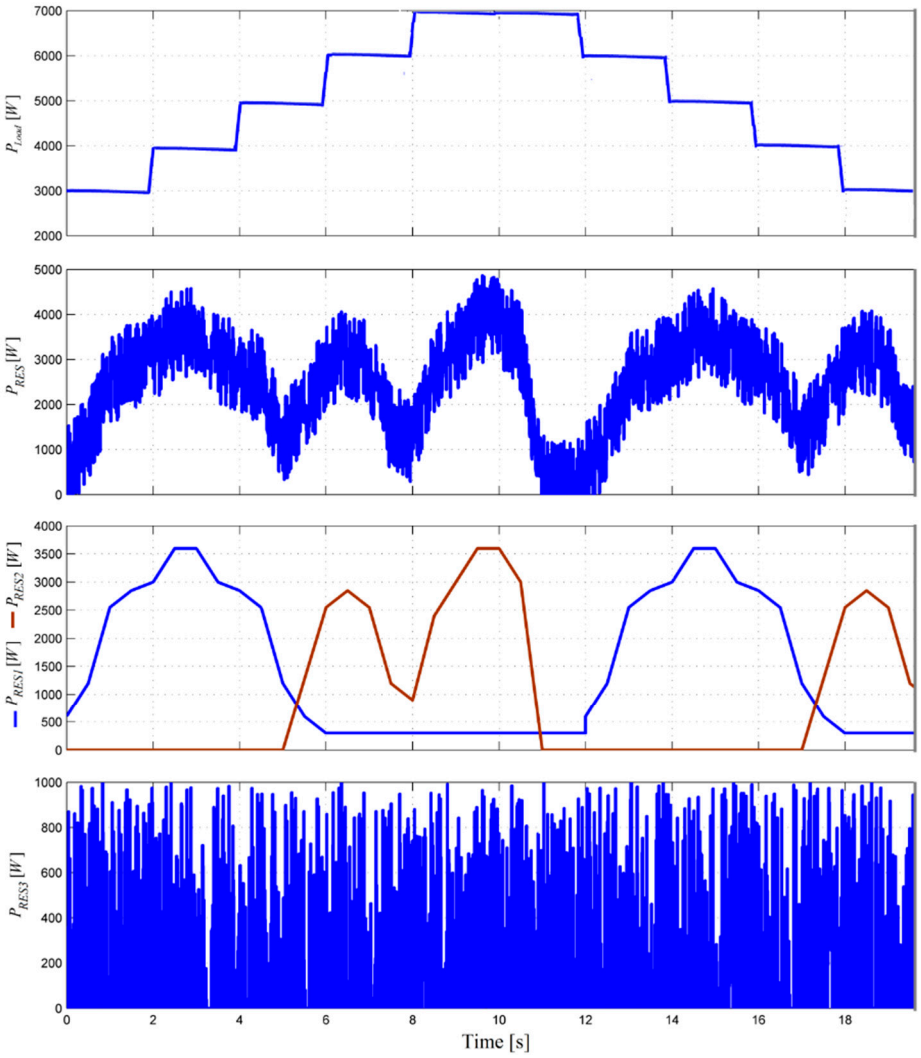

Figure 2. Profiles of the load demand and renewable energy.

A 6 kW FC system (with the slope limits of 100 A/s for the fueling regulators and a 0.2 s time constant) was used as the backup energy source to mitigate the variability of the power flow p_{RES} from the renewable energy sources (RESs) under power-following control (PFC) implemented in the energy management strategy (EMS) unit. This PFC-based strategy operates the battery stack in the charge-sustained mode, avoiding frequent charge-discharge cycles, as is shown below, which will obviously lead to an increase in battery lifespan.

The power flow balance (2) is sustained by a 100 Ah battery with a 100 F ultracapacitor energy storage system (ESS) using a semi-active ESS topology, having the battery on a 200 V DC bus and the ultracapacitors via a bidirectional DC-DC buck–boost converter (see Figure 1):

$$C_{DC}u_{DC}du_{DC}/dt = p_{DC} + p_{RES} + p_{ESS} - p_{Load} \quad (2)$$

where C_{DC} is the capacitor connected on the DC bus.

The power difference on the DC bus, $p_{Load} - p_{RES}$, will be mainly generated by the FC system due to the PFC-based strategy implemented for the fueling regulators. Consequently, the mean value (MV) of the battery's power exchanged with the DC bus is almost zero, except the abrupt transition on load (as it is the case of the load profile chosen in this study):

$$P_{Batt(MV)} \cong 0 \Rightarrow P_{ESS(MV)} \cong 0 \quad (3)$$

This charging mode is very useful in operating a battery stack, increasing the battery lifespan, reducing its size (capacity) and maintenance costs [35,36]. Due to the 20 s time constant of the battery used in simulation, the dynamic compensation of the power balance (2) will be ensured by capacitor C_{DC} of 0.01 F and by 100 F ultracapacitors via the bidirectional DC-DC buck–boost converter controlled by DC voltage regulation loop [37,38].

Thus, considering (3), the MV of the power balance (2) can be written as (4):

$$0 = P_{DC(MV)} + P_{RES(MV)} - P_{Load(MV)} \Rightarrow \eta_{boost} \cdot P_{FCgen} \cong P_{DC(MV)} = P_{Load(MV)} - P_{RES(MV)} \quad (4)$$

The FC power (P_{FCgen}) that is generated on the DC bus is the FC net power (P_{FCnet}):

$$V_{FC} \cdot I_{FC} = P_{FCgen} = P_{FCnet} \cong P_{FC} - P_{cm} \quad (5)$$

where η_{boost} is the efficiency of the DC-DC converter; P_{FC} and $P_{FC(net)}$ is the FC-generated power and FC net power, respectively; and P_{cm} represents the power losses of the air compressor that is modeled using (6) and a 2nd order dynamic system with a 100 Hz natural frequency and 0.7 damping ratio [39,40]:

$$P_{cm} = I_{cm} \cdot V_{cm} = \left(a_2 \cdot AirFr^2 + a_1 \cdot AirFr + a_0\right) \cdot \left(b_1 \cdot I_{FC} + b_0\right) \quad (6)$$

where $a_0 = 0.6$, $a_1 = 0.04$, $a_2 = -0.00003231$, $b_0 = 0.9987$, and $b_1 = 46.02$. Considering (4) and (5), the PFC reference ($I_{ref(PFC)}$) is given by (7):

$$V_{FC} \cdot I_{FC} \cong P_{FC(MV)} \cong \left(P_{Load(MV)} - P_{RES(MV)}\right) / \eta_{boost} \Rightarrow I_{FC} \cong I_{ref(PFC)} = \left(P_{Load(MV)} - P_{RES(MV)}\right) / \left(V_{FC(MV)} \cdot \eta_{boost}\right) \quad (7)$$

A PFC-based strategy of FC net power can be implemented through the boost controller, the air regulator, and the fuel regulator, using the strategy settings block to set an $I_{ref(PFC)}$ reference to one of their references, $I_{ref(Boost)}$, $I_{ref(Air)}$, or $I_{ref(Fuel)}$, respectively (see the EMS unit in Figure 1). The fuel economy-based strategy can be implemented through optimal control based on the global extremum seeking (GES) controller [41–43] (see Figure 1) that generates the $I_{ref(GES)}$ reference by maximizing the multicriteria optimization function (8) that mixes the FC net power (P_{FCnet}) and the fuel consumption efficiency ($Fuel_{eff} = P_{FCnet}/FuelFr$):

$$f(x, AirFr, FuelFr, P_{Load}, P_{RES}) = 0.5 \cdot P_{FCnet} + k_{fuel} \cdot Fuel_{eff} \quad (8)$$

where vector x represents the FC state variables [44,45]; and GES variables $v_1 = AirFr$ and $v_2 = FuelFr$ are the air flow rate ($AirFr$) and the fuel flow rate ($FuelFr$), respectively, given by (9) [46]:

$$AirFr = \frac{60000 \cdot R \cdot (273 + \theta) \cdot N_C \cdot I_{ref(Air)}}{4F \cdot (101325 \cdot P_{f(O2)}) \cdot (U_{f(O2)}/100) \cdot (y_{O2}/100)} \quad (9a)$$

$$FuelFr = \frac{60000 \cdot R \cdot (273 + \theta) \cdot N_C \cdot I_{ref(Fuel)}}{2F \cdot (101325 \cdot P_{f(H2)}) \cdot (U_{f(H2)}/100) \cdot (x_{H2}/100)} \quad (9b)$$

where $N_C, \theta, U_{f(H2)}, U_{f(O2)}, P_{f(H2)}, P_{f(O2)}, x_{H2}, y_{O2}$ are default parameters [47].

P_{Load} and P_{RES} act as a perturbation during the GES-based search of the optimal point, depending on the weighting parameter k_{fuel}, which can be set at zero to maximize P_{FCnet} [48] or at 25 (lpm/W) to reduce the fuel consumption, i.e., $Fuel_T = \int FuelFr(t)dt$ [49,50].

In this study, the DC-DC boost converter was optimally controlled to improve fuel economy, and the PFC-based strategy of the FC net power was implemented through the air regulator or the fuel regulator using the strategies air-PFC or fuel-PFC, respectively, or by both fueling regulators in the switching (SW) strategy (called air/fuel-PFC) that switches the $I_{ref(PFC)}$ reference to the air regulator or the fuel regulator using a power threshold of 5.5 kW for the power requested on the DC bus

($P_{DCreq} = P_{Load} - P_{RES} > 0$). Thus, the strategies air-PFC, fuel-PFC, and air/fuel-PFC are set by (10a), (10b), and (10c) respectively:

$$I_{ref(Fuel)} = I_{FC},\ I_{ref(Air)} = I_{ref(PFC)},\ I_{ref(Boost)} = I_{ref(GES)} \tag{10a}$$

$$I_{ref(Air)} = I_{FC},\ I_{ref(Fuel)} = I_{ref(PFC)},\ I_{ref(Boost)} = I_{ref(GES)} \tag{10b}$$

$$I_{ref(Fuel)} = \begin{cases} I_{ref(PFC)},\ if\ P_{DCreq} \le P_{ref} \\ I_{FC},\ if\ P_{DCreq} > P_{ref} \end{cases} \quad I_{ref(Air)} = \begin{cases} I_{FC},\ if\ P_{DCreq} \le P_{ref} \\ I_{ref(PFC)},\ if\ P_{DCreq} > P_{ref} \end{cases} \quad I_{ref(Boost)} = I_{ref(GES)} \tag{10c}$$

The diagram of FC/ESS renewable HPS using the strategies air-PFC, fuel-PFC, and air/fuel-PFC is presented in Figure 3, and k_{RES} sets the level of RES power on the DC bus. If k_{RES} is zero ($P_{RES} = 0$), then the case of the FC system will be analyzed. If k_{RES} is different to zero, then the case of the FC/renewable HPS will be analyzed. In the last case, if $P_{RES} > P_{Load}$, then the excess of power ($P_{RES} - P_{Load} > 0$) will supply an electrolyzer to produce hydrogen.

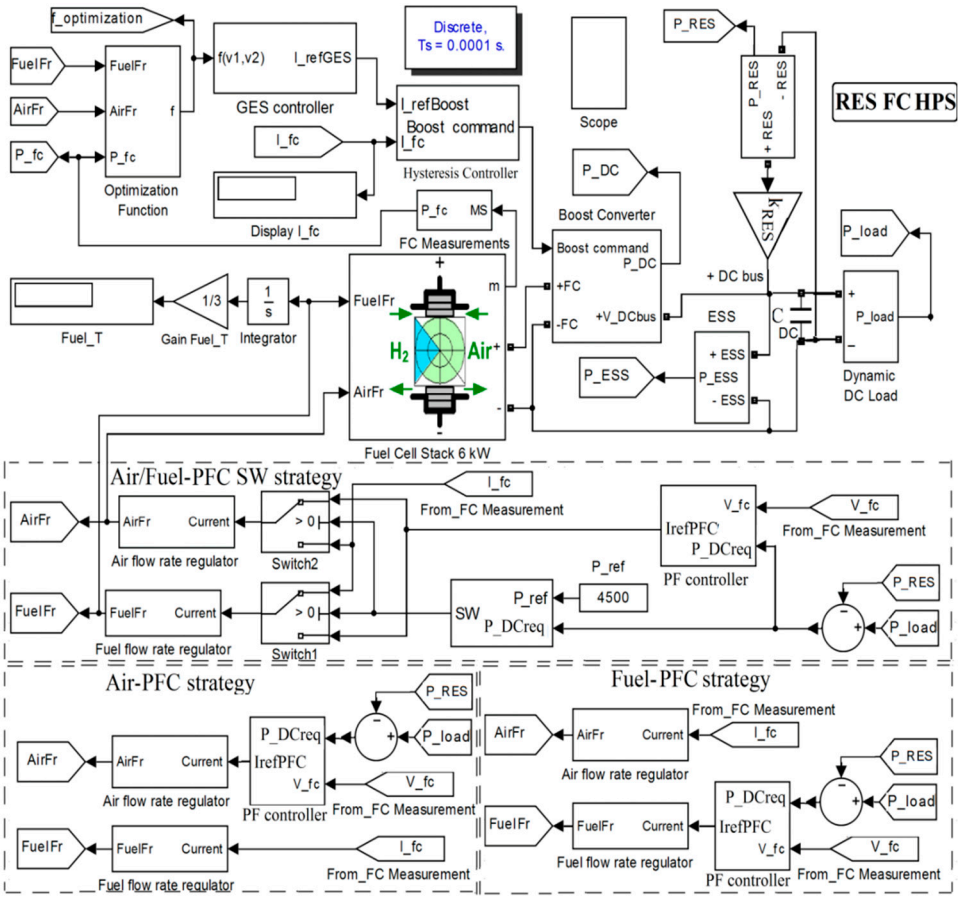

Figure 3. The FC/renewable HPS using power-following control (PFC) strategies air-PFC, fuel-PFC, and air/fuel-PFC [34].

The performance and safe operation of FC/renewable HPS using the strategies air-PFC, fuel-PFC, and air/fuel-PFC is highlighted and compared to the static feed-forward (sFF) control sets by (11) [43]:

$$I_{ref(Fuel)} = I_{FC},\ I_{ref(Air)} = I_{FC},\ I_{ref(boost)} = I_{ref(PFC)} \tag{11}$$

where I_{FC} is the FC current.

The command of the DC-DC boost converter (the signal SW command in Figure 1) is obtained using a 0.1 A hysteresis controller with inputs I_{FC} and $I_{ref(boost)}$.

The GES controller shown in Figure 1 has the following operational relationships [41–43]:

$$y = f(v_1, v_2),\ y_N = k_{Ny} \cdot y \tag{12a}$$

$$\dot{y}_f = -\omega_h \cdot y_f + \omega_h \cdot y_N,\ y_{HPF} = y_N - y_f,\ \dot{y}_{BPF} = -\omega_l \cdot y_{BPF} + \omega_l \cdot y_{HPF} \tag{12b}$$

$$\omega_h = b_h \omega,\ \omega_l = b_l \omega,\ s_d = \sin(\omega t),\ \omega = 2\pi f_d \tag{12c}$$

$$y_{DM} = y_{BPF} \cdot s_d,\ \dot{y}_{Gradient} = y_{DM}, p_1 = k_1 \cdot y_{Gradient} \tag{12d}$$

$$y_M = \left| \frac{1}{T_d} \cdot \int y_{BPF} dt \right|,\quad p_2 = k_2 \cdot y_M \cdot s_d \tag{12e}$$

$$I_{ref(GES)} = k_{Np} \cdot (p_1 + p_2) \tag{12f}$$

where the first harmonic of the FC power (y_{BPF}) is approximated using a band-pass filter with the cut-off frequencies $\omega_l = b_l \omega$ and $\omega_h = b_h \omega$, where $\beta_l = 1.5$ and $\beta_h = 0.1$. This is demodulated with a sinusoidal dither, $s_d = \sin(\omega t)$, and integrated to obtain the search gradient ($y_{Gradient}$), where $\omega = 2\pi f_d$ and f_d = 100 Hz. The search and location signals (p_1 and p_2) are tuned using k_1 and k_2 to speed up tracking of the optimum. In this study, k_1 = 1 and k_2 = 2, and the input and output are normalized using k_{Ny} = 1/1000 and k_{Np} = 20.

It is worth mentioning that after the transitory regime, the stationary values are almost zero [40], resulting in a negligible ripple of FC power and a 99.9% tracking accuracy [43].

OER (λ_{O_2}) is used as an indicator of safe operation of FC/renewable HPS [51]:

$$\lambda_{O_2} = \frac{c_3 \cdot I_{FC}^3 + c_2 \cdot I_{FC}^2 + c_1 \cdot I_{FC} + c_0}{d_1 \cdot I_{FC} + d_0} \tag{13}$$

where $c_0 = 402.6$, $c_1 = 8.476 \cdot 10^{-5}$ $[1/A]$, $c_2 = -0.81252$ $[1/A^2]$, $d_3 = 0.02673$ $[1/A^3]$, $d_0 = 0.997$, and $d_1 = 61.38$. The fuel consumption measured in liters [l] is the performance indicator. This is estimated during 20 s from one minute using (14):

$$Fuel_T = \int FuelFr(t) dt \tag{14}$$

Because *FuelFr* is measured in liters per minute (Lpm), a gain of 1/3 (= 20 s/60 s) is requested to compute the fuel consumption (Gain Fuel_T in Figure 3).

3. Results

The performances of the strategies air-PFC, fuel-PFC, and air/fuel-PFC are compared to the sFF benchmark, starting with the FC system and then with the FC/renewable HPS.

3.1. FC system

3.1.1. Fuel Consumption

The behavior of the FC system using the strategies sFF, air-PFC, fuel-PFC, and air/fuel-PFC is presented in Figures 4–7 under the same load profile (see the 1st plot).

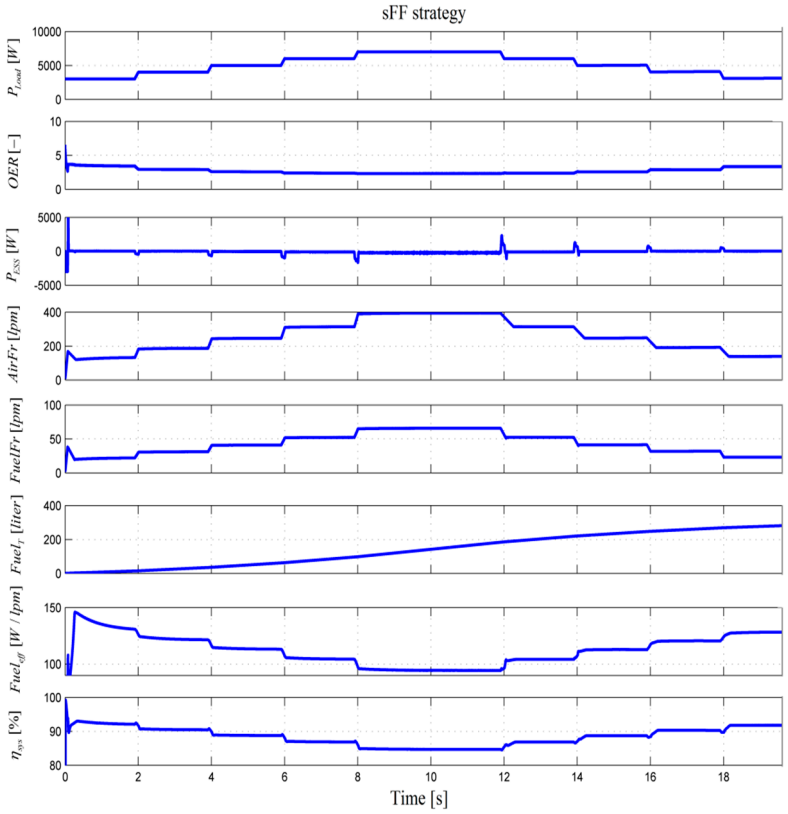

Figure 4. FC system behavior using static feed-forward (sFF) strategy.

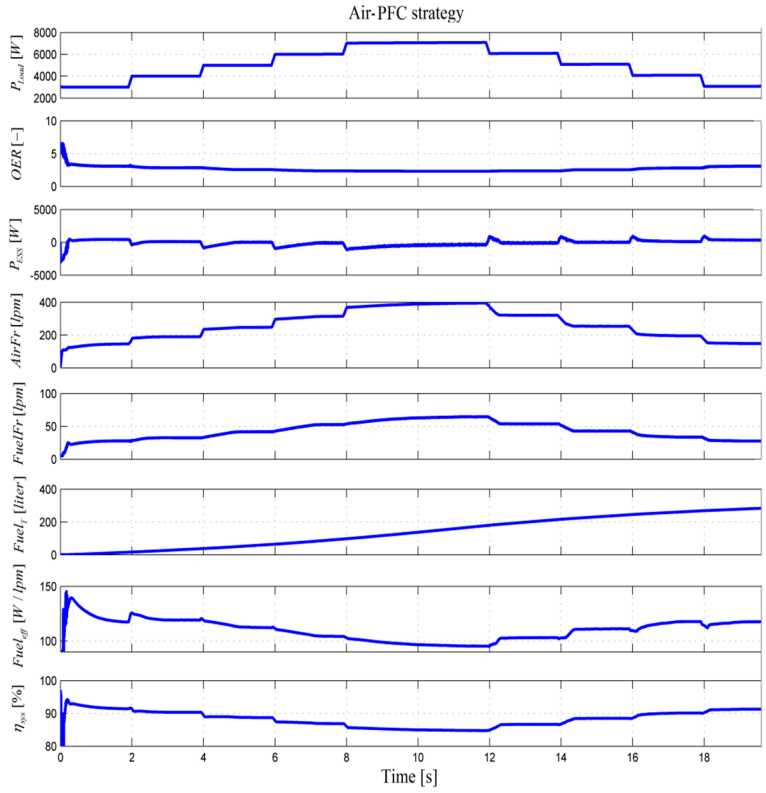

Figure 5. FC system behavior using air-PFC strategy [34].

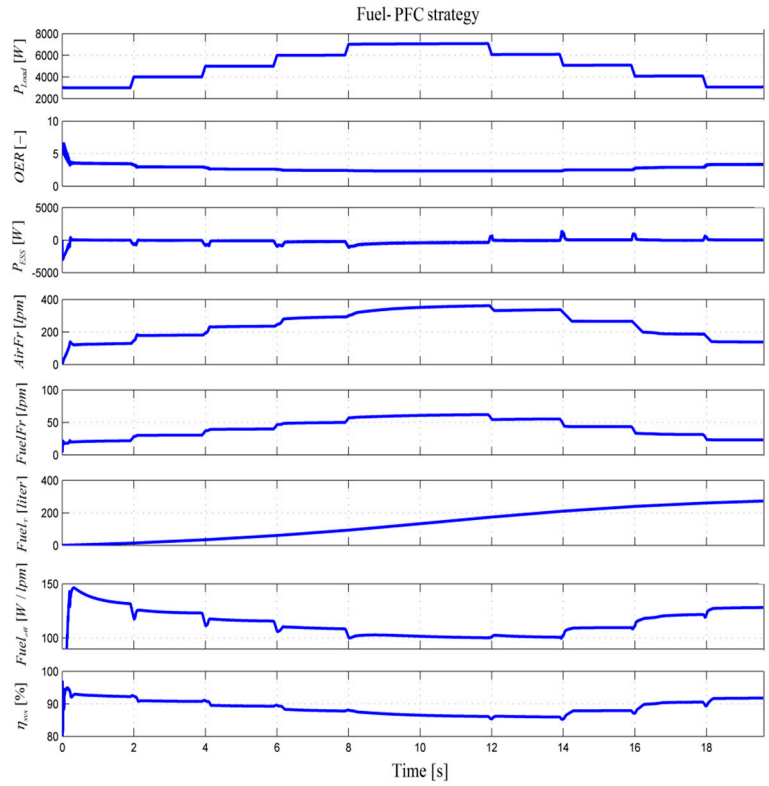

Figure 6. FC system behavior using fuel-PFC strategy [34].

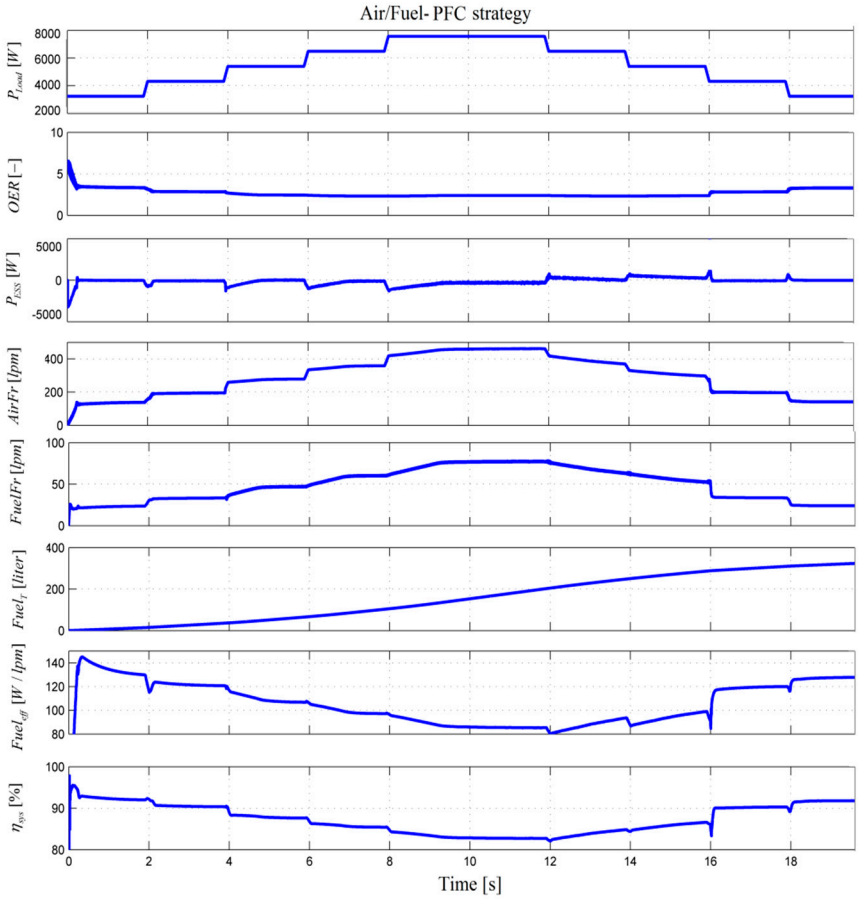

Figure 7. FC system behavior using air/fuel-PFC strategy.

The plots of Figures 4–7 represent the same waveforms as follows: the 1st plot shows the DC load profile; the 2nd plot, OER; the 3rd plot, ESS power; the 4th and 5th plots, *AirFr* and *FuelFr*, respectively; the 6th plot, $Fuel_T$; the 7th plot, $Fuel_{eff}$; and the 8th plot, $\eta_{sys} = P_{FCnet}/P_{FC}$.

OER varies under the recommended limits for all strategies (see the 2nd plot), but minor differences appear due to the specific operation under each strategy (see the next sections). P_{ESS} is almost zero (see the 3rd plot), except the load transitions, validating the charge-sustaining mode of the battery.

The load profile is followed by the both *AirFr* and *FuelFr* in the sFF strategy, then by *AirFr* and *FuelFr* in the strategies air-PFC and fuel-PFC respectively, and by *FuelFr* and then by *AirFr* in the air/fuel-PFC switching strategy (see plots 4 and 5).

The fuel consumption of the FC system using the strategies sFF, air-PFC, fuel-PFC, and air/fuel-PFC is mentioned in Table 1 (see the 6th plot). The last two plots show the variations of the performance indicators $Fuel_{eff}$ and η_{sys}. It should be noted that the ranges of variation for $Fuel_{eff}$ and η_{sys} using the air/fuel-PFC strategy are the same as those using the strategy air-PFC for $P_{Load} > P_{ref}$ and the strategy fuel-PFC for $P_{Load} \leq P_{ref}$, respectively.

Table 1. Fuel consumption of the FC system using the strategies sFF, air-PFC, fuel-PFC, and air/fuel-PFC [34].

$Fuel_{T(sFF)}$	$Fuel_{T(Air\text{-}PFC)}$	$Fuel_{T(Fuel\text{-}PFC)}$	$Fuel_{T(Air/Fuel\text{-}PFC)}$
286.5 L	268.1 L	270.8 L	250.4 L

The fuel economy of the strategy air/fuel-PFC compared to the strategies sFF, air-PFC, and fuel-PFC is estimated in Table 2 using (15):

$$\%Fuel_{T(sFF)} = 100 \cdot \left(\frac{Fuel_{T(sFF)} - Fuel_{T(Air/Fuel-PFC)}}{Fuel_{T(sFF)}} \right) \quad (15a)$$

$$\%Fuel_{T(Air-PFC)} = 100 \cdot \left(\frac{Fuel_{T(Air-PFC)} - Fuel_{T(Air/Fuel-PFC)}}{Fuel_{T(Air-PFC)}} \right) \quad (15b)$$

$$\%Fuel_{T(Fuel-PFC)} = 100 \cdot \left(\frac{Fuel_{T(Fuel-PFC)} - Fuel_{T(Air/Fuel-PFC)}}{Fuel_{T(Fuel-PFC)}} \right) \quad (15c)$$

Table 2. Fuel economy of the FC system using strategy air/fuel-PFC compared to the strategies sFF, air-PFC, and fuel-PFC.

$\%Fuel_{T(sFF)}$	$\%Fuel_{T(Air\text{-}PFC)}$	$\%Fuel_{T(Fuel\text{-}PFC)}$
12.60 L	6.60 L	7.53 L

3.1.2. FC Net Power and Electrical Efficiency

FC electrical efficiency, $\eta_{sys} = P_{FCnet}/P_{FC}$, varied in the range of 82% to 92% for all used strategies analyzed in this paper (Figure 8). The low and high values were obtained for large and light loads, respectively. Higher values can be obtained using $k_{fuel} = 0$ in the optimization function (9) because the objective is the maximization of P_{FCnet}. The air/fuel-PFC strategy uses the power threshold P_{ref} to switch between the strategies air-PFC and fuel-PFC.

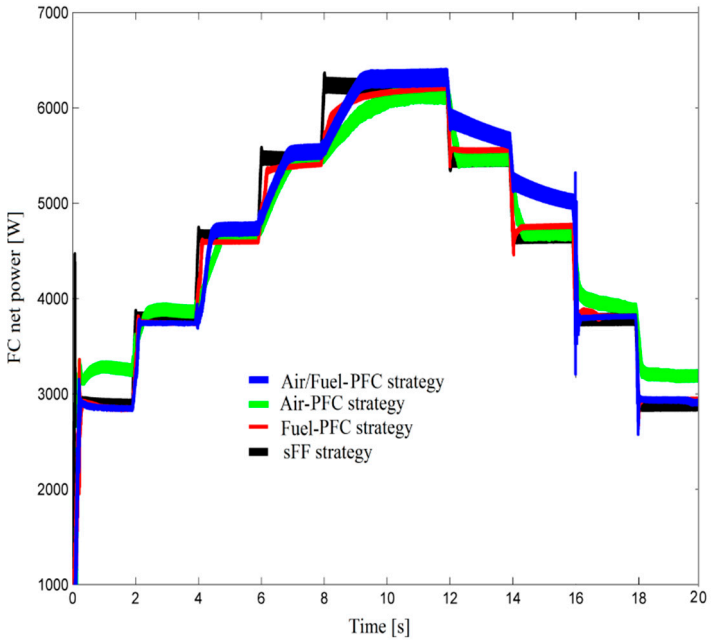

Figure 8. FC net power [34].

Thus, P_{FCnet} levels using the air/fuel-PFC strategy for $P_{Load} \leq P_{ref}$ are close to those of the fuel-PFC strategy and different than those of the air-PFC strategy, especially at light load (see Figure 8). However, the P_{FCnet} levels using the air/fuel-PFC strategy for $P_{Load} > P_{ref}$ and the air-PFC strategy are slightly different due to different initial conditions for the FC system operated under the strategies air/fuel-PFC and air-PFC. The P_{FCnet} levels using the sFF strategy are very close to those using the air/fuel-PFC strategy.

3.1.3. Oxygen Excess Ratio

The OER of the FC system using the strategies sFF, air-PFC, fuel-PFC, and air/fuel-PFC is shown in Figure 9.

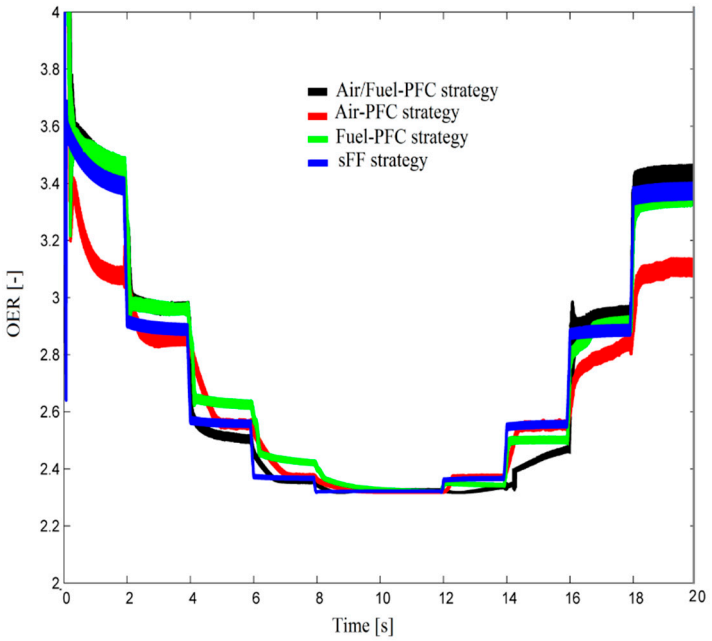

Figure 9. Oxygen excess ratio [34].

The air/fuel-PFC strategy uses the power threshold P_{ref} to switch between the strategies air-PFC and fuel-PFC. In this way, the OER levels using the air/fuel-PFC strategy for $P_{Load} \leq P_{ref}$ are close to those of the strategies fuel-PFC and sFF, but different than those of the air-PFC strategy (see Figure 9). For all the strategies analyzed, the OER levels for the FC system operated near the maximum power were close to each other. In any case, for any level and transition in the load profile, the OER varies within the safe limits (from 2.3 to 4), ensuring a safe operation of the FC power system [43,45,50].

The results obtained for the FC system and battery stack are validated in next section for FC/renewable HPS.

3.2. FC/Renevable Hybrid Power System

3.2.1. Fuel Consumption

The behavior of the FC/renewable HPS using the strategies sFF, air-PFC, fuel-PFC, and air/fuel-PFC are presented in Figures 10–13 under the same load profile (see the 1st plot), but using the profile of renewable energy presented in Figure 2 and is seen here in the 2nd plot.

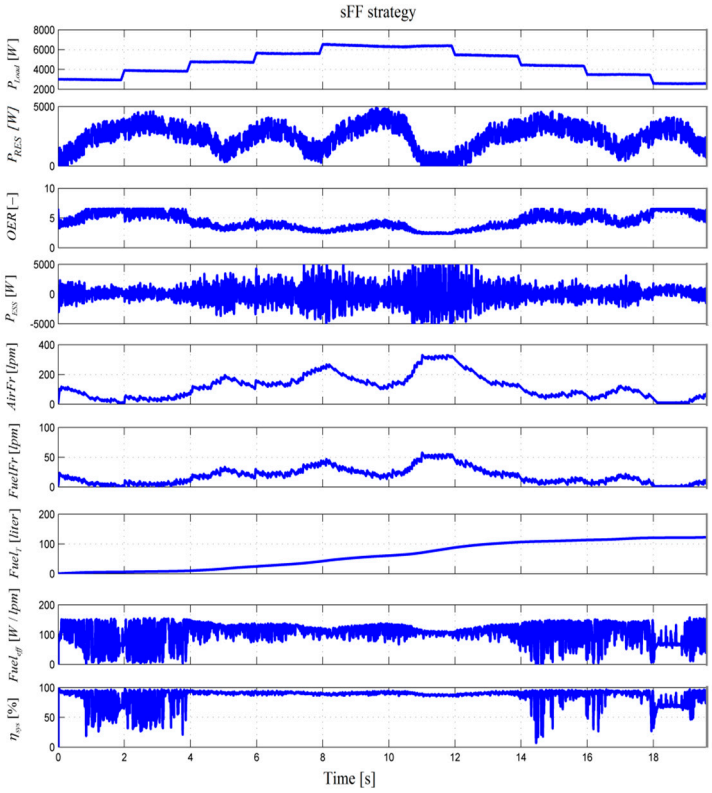

Figure 10. FC/renewable HPS behavior using sFF strategy.

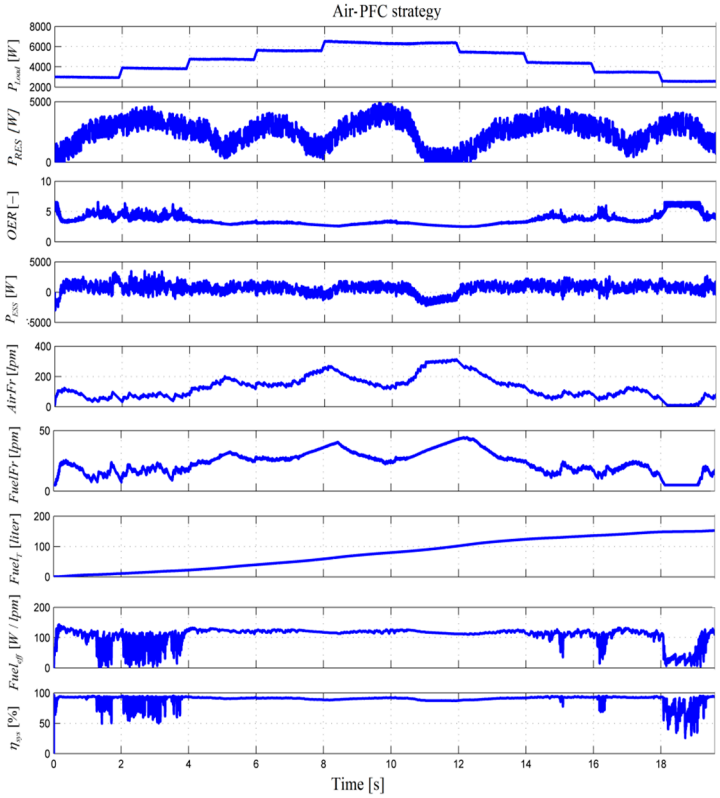

Figure 11. FC/renewable HPS behavior using the air-PFC strategy.

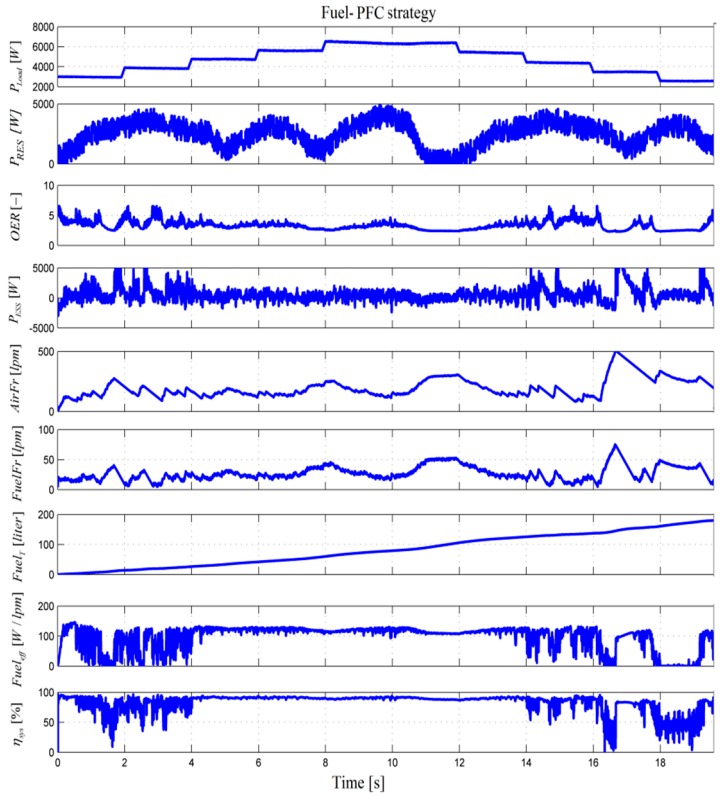

Figure 12. FC/renewable HPS behavior using the fuel-PFC strategy.

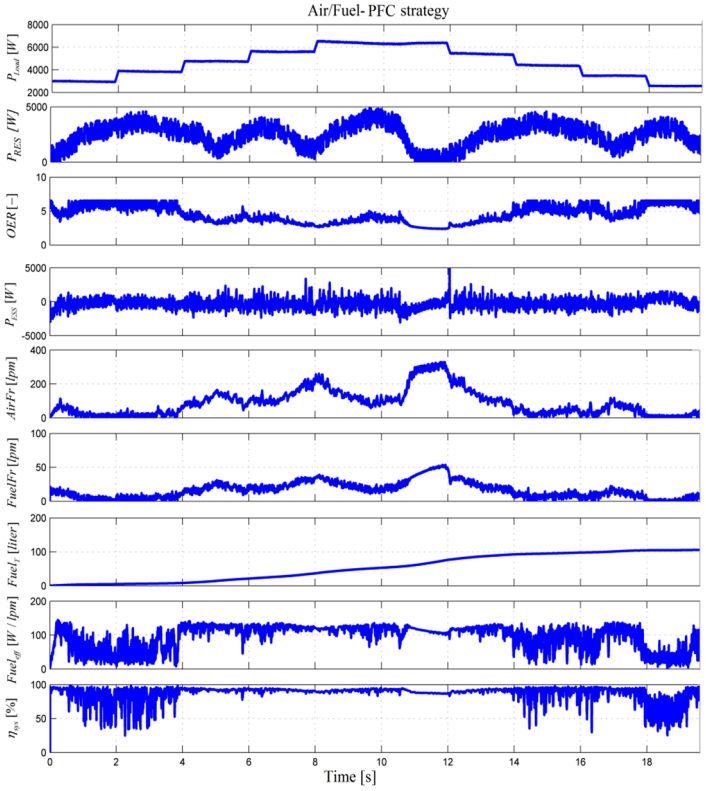

Figure 13. FC/renewable HPS behavior using air/fuel-PFC strategy.

It can be seen that the structure of the plots in Figures 10–13 are the same as that of Figures 4–7, with the exception of adding RES power in the 2nd plot, being as follows: the 1st plot shows the DC load profile; the 2nd plot, RES power; the 3rd plot, OER; the 4th plot, ESS power; the 5th and 6th plots, *AirFr* and *FuelFr*, respectively; the 7th plot, $Fuel_T$; the 8th plot, $Fuel_{eff}$; and the 9th plot, $\eta_{sys} = P_{FCnet}/P_{FC}$. The OER of the FC/renewable HPS under all strategies varies in a large range (from 2.3 to 7) compared to the OER of the FC system (from 2.3 to 4), but it still is under recommended limits (see the 3rd plot).

It can be seen that P_{ESS} still varies around zero but is noisy due to the random part added to renewable energy (see the 4th plot), thus validating the charge-sustaining mode of the battery in the case of FC/renewable HPS.

The power profile $P_{Load} - P_{RES} > 0$ is followed by the both *AirFr* and *FuelFr* in the sFF strategy, by *AirFr* and *FuelFr* in the strategies air-PFC and fuel-PFC respectively, and by *FuelFr* and then by *AirFr* in the air/fuel-PFC switching strategy (see plots 5 and 6). If $P_{RES} - P_{Load} > 0$, then the FC system operates in standby mode, and the excess of power ($P_{RES} - P_{Load}$) will supply an electrolyzer to produce hydrogen.

The fuel consumption of the FC system using the strategies sFF, air-PFC, fuel-PFC and air/fuel-PFC is mentioned in Table 3 (see the 7th plot). The last two plots show the values of the performance indicators $Fuel_{eff}$ and η_{sys}. It should be noted that the values of $Fuel_{eff}$ and η_{sys} are lower due to the standby mode of the FC system operation in the case where RES power exceeds the load demand ($P_{RES} > P_{Load}$).

Table 3. Fuel consumption of FC/renewable HPS using the strategies sFF, air-PFC, fuel-PFC, and air/fuel-PFC.

$Fuel^{Renewable}_{T(Air/Fuel\text{-}PFC)}$	$Fuel^{Renewable}_{T(Air\text{-}PFC)}$	$Fuel^{Renewable}_{T(Fuel\text{-}PFC)}$	$Fuel^{Renewable}_{T(sFF)}$
107 L	115.4 L	116.6 L	123.6 L

The fuel economy of the strategy air/fuel-PFC compared to the strategies sFF, air-PFC, and fuel-PFC is estimated in Table 4 using (16):

$$\%Fuel^{Renewable}_{T(sFF)} = 100 \cdot \left(\frac{Fuel^{Renewable}_{T(sFF)} - Fuel^{Renewable}_{T(Air/Fuel-PFC)}}{Fuel^{Renewable}_{T(sFF)}} \right) \quad (16a)$$

$$\%Fuel^{Renewable}_{T(Air-PFC)} = 100 \cdot \left(\frac{Fuel^{Renewable}_{T(Air-PFC)} - Fuel^{Renewable}_{T(Air/Fuel-PFC)}}{Fuel^{Renewable}_{T(Air-PFC)}} \right) \quad (16b)$$

$$\%Fuel^{Renewable}_{T(Fuel-PFC)} = 100 \cdot \left(\frac{Fuel^{Renewable}_{T(Fuel-PFC)} - Fuel^{Renewable}_{T(Air/Fuel-PFC)}}{Fuel^{Renewable}_{T(Fuel-PFC)}} \right) \quad (16c)$$

Table 4. Fuel economy of FC/renewable HPS using the strategy air/fuel-PFC compared to the strategies sFF, air-PFC, and fuel-PFC.

$\%Fuel^{Renewable}_{T(Air\text{-}PFC)}$	$\%Fuel^{Renewable}_{T(Fuel\text{-}PFC)}$	$\%Fuel^{Renewable}_{T(sFF)}$
7.28 L	8.23 L	13.43 L

3.2.2. FC Net Power and Electrical Efficiency

The P_{FCnet} levels using all strategies (see Figure 14) vary from about 0.1 kW (standby operating mode) to 6 kW (nominal operating mode).

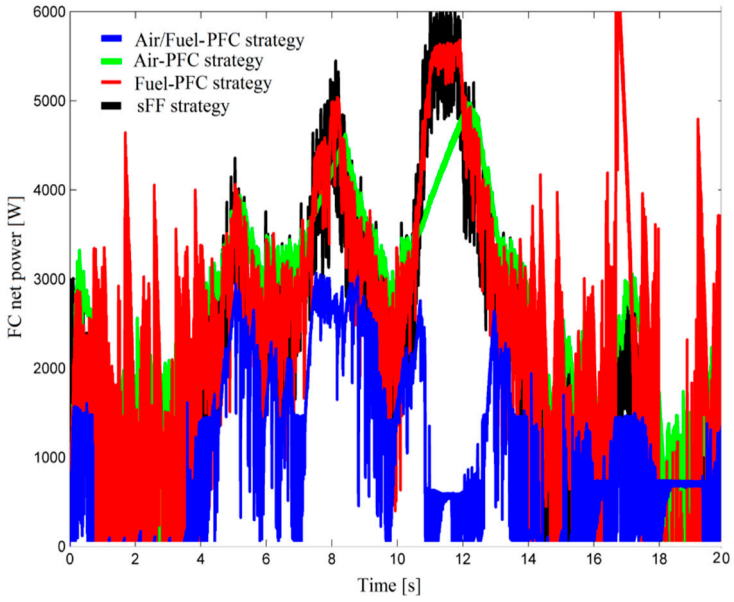

Figure 14. FC net power.

To avoid having many start-stop occurrences in the FC system, the standby operating mode was chosen, but an appropriate strategy to supply the electrolyzer during the stages when $P_{RES} > P_{Load}$ must be used.

3.2.3. Oxygen Excess Ratio

Because P_{FCnet} varies in the range of 0.1 to 6 kW for the FC system and from 2.8 to 6.5 kW for FC/renewable HPS, the OER will vary in a large range for FC/renewable HPS (from about 2.3 to 7) but is still within the safe limits (see Figure 15).

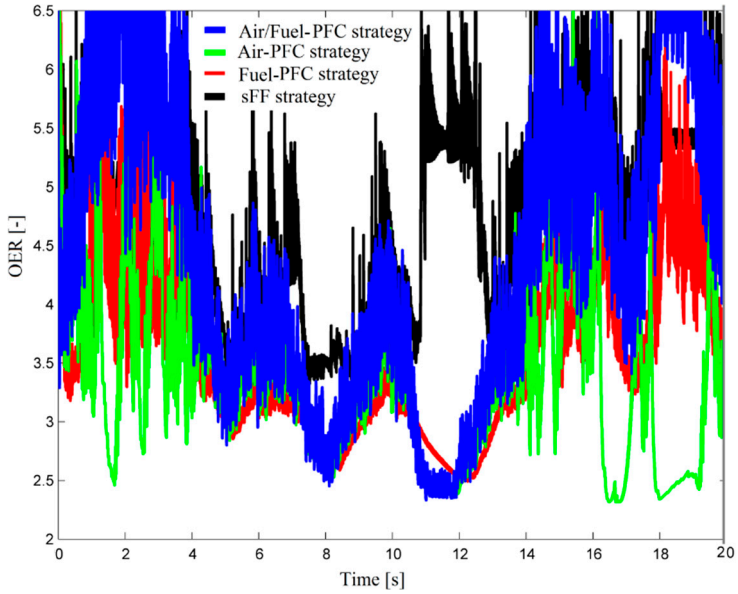

Figure 15. Oxygen excess ratio.

4. Discussion

The results were comparatively analyzed in section of the results for the FC system and the FC/renewable HPS using the strategies sFF, air-PFC, fuel-PFC, and air/fuel-PFC; here, we summarize and discuss these further in the frame of the working hypotheses.

The fuel consumption using the strategies sFF, air-PFC, fuel-PFC, and air/fuel-PFC for the FC system and the FC/renewable HPS is summarized in Table 5.

Table 5. Comparison of the fuel consumption using the strategies sFF, air-PFC, fuel-PFC, and air/fuel-PFC for the FC system and FC/renewable HPS.

Parameter [unit] \ Strategy	sFF	Air-PFC	Fuel-PFC	Air/Fuel-PFC
$Fuel_{T(strategy)}$ [L]	286.5	268.1	270.8	250.4
$Fuel^{Renewable}_{T(strategy)}$ [L]	107	115.4	116.6	123.6
$Fuel_{T(strategy)} - Fuel^{Renewable}_{T(strategy)}$ [L]	143.40	152.70	154.20	162.90
$\left(Fuel_{T(strategy)} - Fuel^{Renewable}_{T(strategy)}\right) / Fuel_{T(strategy)}$ [%]	57.27	56.96	56.94	56.86

It is worth mentioning that the lowest fuel consumption was obtained using the air/fuel-PFC strategy for both FC-based power systems and then by using the strategies air-PFC, fuel-PFC, and sFF (see the first two rows of Table 5).

In addition, it should be noted that the difference in the fuel consumption for the FC system and FC/renewable HPS, $Fuel_{T(strategy)} - Fuel^{Renewable}_{T(strategy)}$, represents about 57% of the fuel consumption of the FC system using that strategy (see the last row of Table 5).

This difference results from operating the FC system from the FC/renewable HPS at low power due to contribution of RES power on the load demand. The profiles of the load demand and RES power shown in Figure 2 have a MV of 5 kW and about 2.5 kW, justifying the 57% reduction in the fuel consumption for the FC system and FC/renewable HPS.

The fuel economy strategies for the FC/renewable HPS compared to the FC system are better by about 0.7% (see last row of Table 6) due to the same reason (FC system operates at lower power due to available renewable energy on the DC bus).

Table 6. Fuel economy of the FC system and FC/renewable HPS using the strategy air/fuel-PFC compared to the strategies sFF, air-PFC, and fuel-PFC.

Parameter [unit] \ Strategy	sFF	Air-PFC	Fuel-PFC
$\%Fuel_{T(strategy)}$ [%]	6.60	7.53	12.60
$\%Fuel^{Renewable}_{T(stategy)}$ [%]	7.28	8.23	13.43
$\%Fuel^{Renewable}_{T(stategy)} - \%Fuel_{T(stategy)}$ [%]	0.68	0.70	0.83

5. Conclusions

This paper performed a systematic evaluation of the strategies referred to as air/fuel-PFC, air-PFC, fuel-PFC, and sFF, with the latter being a commercial benchmark used in the analysis of the obtained results. The following findings resulted for FC system (FC/ESS/RES HPS with $P_{RES} = 0$):

- The four strategies mentioned above were analyzed as the performance and safe operation of the FC system and battery pack using indicators such as fuel economy and OER.
- Following the analysis, the fuel economy strategies for the FC system were ordered starting with the best strategy: air/fuel-PFC, air-PFC, fuel-PFC, and sFF.
- The percentage of hydrogen economy for an air/fuel-PFC strategy compared to the strategies sFF, air-PFC, and fuel-PFC is 6.60%, 7.53%, and 12.60% of the total hydrogen consumption of these strategies (see Table 2).
- FC net power is generated based on the power flow balance (2) and on a PFC-based strategy to operate the battery in charge-sustained mode (see the 3rd plot in Figures 4–8), increasing their lifespan.
- OER varies within the safe limits (see Figure 9).

The results obtained for the FC system and battery pack were validated for an FC/ESS/RES HPS with $P_{RES} > 0$, producing the following findings:

- From point of view of the hydrogen economy, the same order of the strategies were obtained for an FC/renewable HPS: air/fuel-PFC, air-PFC, fuel-PFC, and sFF.
- The integration of the FC system into a renewable HPS will increase with 0.7% of the fuel economy of the air/fuel-PFC strategy for the FC/renewable HPS compared to the FC system (see last row of Table 6) due to the FC system operating at lower power when the renewable energy is available.
- PFC-based strategies still operate the battery pack in the charge-sustained mode (see the 4th plot in Figures 10–13) even under variable RES power, increasing battery lifespan.
- OER still varies within the safe limits (see Figure 15).

Thus, the novelty and contribution of this paper can be summarized as follows:

- The use of a PFC-based strategy will establish the FC-system fueling flows so that FC net power compensates the balance of power flows on the DC bus using a battery stack with lower capacity than in other strategies proposed in the literature due to the battery pack operating in charge-sustained mode. The next work will analyze whether only the ultracapacitors pack can dynamically compensate the power flow balance via a bidirectional DC-DC power converter.
- The maximization of the fuel economy was obtained by using a real-time optimal control of the boost power converter.
- The operation of FC system under a PFC-based strategy and optimal fuel economy control is done in safe operating conditions, maintaining OER within the safe limits.

However, before implementing the air/fuel-PFC strategy, these findings should be validated by several future studies using different profiles of charging demand and renewable energy.

Author Contributions: Conceptualization, methodology, and writing—Original draft preparation: N.B. and P.T.; validation: M.C., M.I., and M.O.; supervision: M.V. and E.C.; formal analysis: N.B. and P.T.; writing—Review and editing: N.B., M.S.R., and I.S.S. All authors have read and agreed to the published version of the manuscript.

Funding: This work was partially supported by the International Research Partnerships: Electrical Engineering Thai- French Research Center (EE-TFRC) between King Mongkut's University of Technology North Bangkok and Université de Lorraine under Grant KMUTNB−BasicR−64−17.

Acknowledgments: This work was carried out through the Nucleus Program, financed by the Ministry of Education and Research, Romania, project no. PN 19 11 02 02, "Innovative solution for testing and validating fuel cell systems in automotive applications" and project number PN-III-P1-1.2-PCCDI-2017-0194/25 PCCDI within PNCDI III.

Conflicts of Interest: The authors declare no conflict of interest.

Nomenclature

Abbreviations:

Air-PFC	Strategy based on the control of the air regulator
Air/Fuel-PFC	Strategy based on the control of the air regulator and the fuel regulator
AV	Average value
EMS	Energy management strategy
EMU	Energy management unit
ES	Extremum seeking
ESS	Energy storage system
GES	Global extremum seeking
Fuel-PFC	Strategy based on the control of the fuel regulator
FC	Fuel cell
FCHPS	Fuel cell hybrid power systems
HPS	Hybrid power system
LPM	Liter per minute
LFW	Load following
MEA	Membrane electrode assembly
MEP	Maximum efficiency point
MPP	Maximum power point
MV	Mean value
PEMFC	proton exchange membrane fuel cell
PFC	Power-following control
OER	Oxygen excess ratio
RES	Renewable energies source
sFF	Static feed-forward
SoC	State-of-charge
SW	Switch
UC	Ultracapacitor

Symbols:

$AirFr$	Airflow rate
C_{DC}	Capacitor DC
f_d	Dither frequency
F	Faraday constant
$Fuel_{eff}$	Fuel consumption efficiency
$Fuel_{Fr}$	Fuel flow rate
$Fuel_T$	Total fuel consumption
k_{fuel}	Weighting coefficient of the fuel consumption efficiency
k_{net}	Weighting coefficient of the FC net power
k_{Ny}	Normalization gain
k_{RES}	Constant for RES
I_{cm}	Air compressor current

I_{FC}	FC stack current
$I_{ref(Air)}$	Air flow reference
$I_{ref(Boost)}$	Boost converter reference
$I_{ref(Fuel)}$	Fuel flow reference
$I_{ref(GES)}$	GES reference
$I_{ref(PFC)}$	PFC reference
N_c	Number of cells in series
$P_{f(H2)}$	Pressure of the fuel
$P_{f(O2)}$	Pressure of the air
P_{DCreq}	Power requested on the DC bus
P_{FC}	FC stack power
P_{DC}	Power on the DC bus
P_{Load}	Variable load power
R	Universal gas constant
v_1, v_2	Variable for the reactant flow rate optimum
V_{cm}	Air compressor voltage
V_{FC}	FC stack voltage
u_{DC}	DC bus voltage
$U_{f(H2)}$	Nominal utilization of hydrogen
$U_{f(O2)}$	Nominal utilization of oxygen
y_{BF}	First harmonic of the FC power
y_{O2}	Composition of oxidant
x_{H2}	Composition of fuel
θ	Operating temperature
η_{sys}	FC electrical efficiency
η_{boost}	FC boost converter efficiency

References

1. Masson-Delmotte, V.; Zhai, P.; Pörtner, H.-O.; Roberts, D.; Skea, J.; Shukla, P.R.; Pirani, A.; Moufouma-Okia, W.; Péan, C.; Pidcock, R.; et al. (Eds.) *Global Warming of 1.5 °C. An IPCC Special Report on the Impacts of Global Warming of 1.5 °C above Pre-Industrial Levels and Related Global Greenhouse Gas Emission Pathways, in the Context of Strengthening the Global Response to the Threat of Climate Change, Sustainable Development, and Efforts to Eradicate Poverty*; Intergovernmental Panel on Climate Change (IPCC): Geneva, Switzerland, 2019. Available online: https://www.ipcc.ch/site/assets/uploads/sites/2/2019/06/SR15_Full_Report_High_Res.pdf (accessed on 29 October 2020).
2. Kempener, R.; Lavagne, O.; Saygin, D.; Skeer, J.; Vinci, S.; Gielen, D. *Off-Grid Renewable Energy Systems: Status and Methodological Issues*; International Renewable Energy Agency (IRENA): Abu Dhabi, UAE, 2015. Available online: https://www.irena.org/-/media/Files/IRENA/Agency/Publication/2015/IRENA_Off-grid_Renewable_Systems_WP_2015.pdf (accessed on 29 October 2020).
3. *Global Energy Review*; International Energy Agency (IEA): Paris, France, 2020. Available online: https://www.iea.org/reports/global-energy-review-2020 (accessed on 29 October 2020).
4. Mahomed, E.-S. Operational Characteristics of Renewable Sources, Challenges, and Future Prospective. In *Economics of Variable Renewable Sources for Electric Power Production*; Lambert Academic Publishing: Saarbrücken, Germany, 2017.
5. Arabul, F.K.; Arabul, A.Y.; Kumru, C.F.; Boynuegri, S.R. Providing energy management of a fuel cell- battery-wind turbine- solar panel hybrid off grid smart home system. *Int. J. Hydrogen Energy* **2017**, *42*, 26906–26913.
6. Azarpour, A.; Suhaimi, S.; Zahedi, G.; Bahadori, A. A Review on the Drawbacks of Renewable Energy as a Promising Energy Source of the Future. *Arab. J. Sci. Eng.* **2013**, *38*, 317–328.
7. Ghenai, C.; Bettayeb, M.; Brdjanin, B.; Hamid, A.K. Hybrid solar PV/PEM fuel Cell/Diesel Generator power system for cruise ship: A case study in Stockholm, Sweden. *Case Stud. Therm. Eng.* **2019**, *14*, 100497. [CrossRef]

8. Bizon, N. *Optimization of the Fuel Cell Renewable Hybrid Power Systems*; Springer: London, UK, 2020.
9. Staffell, I.; Scamman, D.; Abad, A.V.; Balcombe, P.; Dodds, P.E.; Ekins, P.; Shah, N.; Ward, K.R. The role of hydrogen and fuel cells in the global energy system. *Energy Environ. Sci.* **2019**, *12*, 463–491.
10. Barbir, F. *PEM Fuel Cells: Theory and Practice*, 2nd ed.; Academic Press: Cambridge, UK, 2013.
11. Sanka, K.; Jana, A.K. Nonlinear multivariable sliding mode control of a reversible PEM fuel cell integrated system. *Energy Convers. Manag.* **2018**, *171*, 541–565.
12. Zhang, Z.; Miyajima, R.; Inada, T.; Miyagi, T.; Tsuda, M. Novel energy management method for suppressing fuel cell degradation in hydrogen and electric hybrid energy storage systems compensating renewable energy fluctuations. *Int. J. Hydrogen Energy* **2018**, *43*, 6879–6886.
13. Bizon, N. Load-following Mode Control of a Standalone Renewable/Fuel Cell Hybrid Power Source. *Energy Convers. Manag.* **2014**, *77*, 763–772.
14. Sikkabut, S.; Mungporn, P.; Ekkaravarodome, C.; Bizon, N.; Tricoli, P.; Nahid-Mobarakeh, B.; Pierfederici, S.; Davat, B.; Thounthong, P. Control of High-Energy High-Power Densities Storage Devices by Li-ion Battery and Supercapacitor for Fuel Cell/Photovoltaic Hybrid Power Plant for Autonomous System Applications. *IEEE Trans. Ind. Appl.* **2016**, *52*, 4395–4407.
15. Bizon, N. Effective Mitigation of the Load Pulses by Controlling the Battery/SMES Hybrid Energy Storage System. *Appl. Energy* **2018**, *229*, 459–473.
16. Yang, B.; Wang, J.; Zhang, X.; Wang, J.; Shu, H.; Li, S.; He, T.; Lan, C.; Yu, T. Applications of battery/supercapacitor hybrid energy storage systems for electric vehicles using perturbation observer based robust control. *J. Power Sources* **2020**, *448*, 22744. [CrossRef]
17. Nadeem, F.; Hussain, S.S.; Tiwari, P.K.; Goswami, A.K.; Ustun, T.S. Comparative Review of Energy Storage Systems, Their Roles, and Impacts on Future Power Systems. *IEEE Access* **2019**, *7*, 4555–4585.
18. Li, H.; Ravey, A.; N'Diaye, A.; Djerdir, A. Online adaptive equivalent consumption minimization strategy for fuel cell hybrid electric vehicle considering power sources degradation. *Energy Convers. Manag.* **2019**, *192*, 133–149.
19. Lü, X.; Wu, Y.; Lian, J.; Zhang, Y.; Chen, C.; Wang, P.; Meng, L. Energy management of hybrid electric vehicles: A review of energy optimization of fuel cell hybrid power system based on genetic algorithm. *Energy Convers. Manag.* **2020**, *205*, 112474. [CrossRef]
20. Yue, M.; Jemei, S.; Gouriveau, R.; Zerhouni, N. Review on health-conscious energy management strategies for fuel cell hybrid electric vehicles: Degradation models and strategies. *Int. J. Hydrogen Energy* **2019**, *44*, 6844–6861.
21. Sun, Z.; Wang, Y.; Chen, Z.; Li, X. Min-max game based energy management strategy for fuel cell/supercapacitor hybrid electric vehicles. *Appl. Energy* **2020**, *267*, 115086.
22. Han, Y.; Chen, W.; Li, Q.; Yang, H.; Zare, F.; Zheng, Y. Two-level energy management strategy for PV-Fuel cell-battery-based DC microgrid. *Int. J. Hydrogen Energy* **2019**, *44*, 19395–19404.
23. Soumeur, M.A.; Gasbaoui, B.; Abdelkhalek, O.; Ghouili, J.; Toumi, T.; Chakar, A. Comparative study of energy management strategies for hybrid proton exchange membrane fuel cell four wheel drive electric vehicle. *J. Power Sources* **2020**, *426*, 228167. [CrossRef]
24. Kandidayeni, M.; Macias, A.; Boulon, L.; Kelouwani, S. Investigating the impact of ageing and thermal management of a fuel cell system on energy management strategies. *Appl. Energy* **2020**, *274*, 115293. [CrossRef]
25. Chang, H.; Xu, X.; Shen, J.; Shu, S.; Tu, Z. Performance analysis of a micro-combined heating and power system with PEM fuel cell as a prime mover for a typical household in North China. *Int. J. Hydrogen Energy* **2019**, *44*, 24965–24976.
26. Wu, W.; Partridge, J.S.; Bucknall, R.W.G. Stabilised control strategy for PEM fuel cell and supercapacitor propulsion system for a city bus. *Int. J. Hydrogen Energy* **2018**, *43*, 12302–12313.
27. Ou, K.; Yuan, W.W.; Choi, M.; Yang, S.; Jung, S.; Kim, Y.B. Optimized power management based on adaptive-PMP algorithm for a stationary PEM fuel cell/battery hybrid system. *Int. J. Hydrogen Energy* **2018**, *43*, 15433–15444.

28. Chen, H.; Liu, B.; Liu, R.; Weng, Q.; Zhang, T.; Pei, P. Optimal interval of air stoichiometry under different operating parameters and electrical load conditions of proton exchange membrane fuel cell. *Energy Convers. Manag.* **2020**, *205*, 112398. [CrossRef]
29. Yuan, H.; Dai, H.; Wei, X.; Ming, P. Model-based observers for internal states estimation and control of proton exchange membrane fuel cell system: A review. *J. Power Sources* **2020**, *46831*, 228376. [CrossRef]
30. Huang, Y.; Wang, H.; Khajepour, A.; Li, B.; Ji, J.; Zhao, K.; Hu, C. A review of power management strategies and component sizing methods for hybrid vehicles. *Renew. Sustain. Energy Rev.* **2018**, *98*, 132–144.
31. Mihaescu, M. Applications of multiport converters. *J. Electr. Eng. Electron. Control Comput. Sci.* **2016**, *2*, 13–18. Available online: http://jeeeccs.net/index.php/journal/article/view/25 (accessed on 29 October 2020).
32. Das, H.S.; Tan, C.W.; Yatim, A.H.M. Fuel cell hybrid electric vehicles: A review on power conditioning units and Topologies. *Renew. Sustain. Energy Rev.* **2017**, *76*, 268–291.
33. Jyoti Saharia, B.; Brahma, H.; Sarmah, N. A review of algorithms for control and optimization for energy management of hybrid renewable energy systems. *J. Renew. Sustain. Energy* **2018**, *10*, 053502.
34. Oproescu, M.; Bizon, N.; Carcadea, E.; Culcer, M.; Iliescu, M.; Raceanu, M.; Sorlei, S. Performance of the load-following control switched to the air and hydrogen regulators of the fuel cell system. In Proceedings of the 2020 12th International Conference on Electronics, Computers and Artificial Intelligence (ECAI), Bucharest, Romania, 25–27 June 2020. [CrossRef]
35. Sorrentino, M.; Cirillo, V.; Nappi, L. Development of flexible procedures for co-optimizing design and control of fuel cell hybrid vehicles. *Energy Convers. Manag.* **2019**, *185*, 537–551.
36. Pan, Z.F.; An, L.; Wen, C.Y. Recent advances in fuel cells based propulsion systems for unmanned aerial vehicles. *Appl. Energy* **2019**, *240*, 473–485.
37. Etouke, P.O.; Nneme, L.N.; Mbihi, J. An Optimal Control Scheme for a Class of Duty-Cycle Modulation Buck Choppers: Analog Design and Virtual Simulation. *J. Electr. Eng. Electron. Control Comput. Sci.* **2020**, *6*, 13–20. Available online: https://jeeeccs.net/index.php/journal/article/view/142 (accessed on 29 October 2020).
38. Nnem, L.N.; Lonla, B.M.; Sonfack, G.B.; Mbihi, J. Review of a Multipurpose Duty-Cycle Modulation Technology in Electrical and Electronics Engineering. *J. Electr. Eng. Electron. Control Comput. Sci.* **2018**, *4*, 9–18. Available online: https://jeeeccs.net/index.php/journal/article/view/101 (accessed on 29 October 2020).
39. Ramos-Paja, C.A.; Spagnuolo, G.; Petrone, G.; Mamarelis, E. A perturbation strategy for fuel consumption minimization in polymer electrolyte membrane fuel cells: Analysis, Design and FPGA implementation. *Appl. Energy* **2014**, *119*, 21–32.
40. Bizon, N. Fuel saving strategy using real-time switching of the fueling regulators in the Proton Exchange Membrane Fuel Cell System. *Appl. Energy* **2019**, *252*, 113449–113453.
41. Bizon, N.; Thounthong, P.; Raducu, M.; Constantinescu, L.M. Designing and Modelling of the Asymptotic Perturbed Extremum Seeking Control Scheme for Tracking the Global Extreme. *Int. J. Hydrogen Energy* **2017**, *42*, 17632–17644.
42. Bizon, N. Searching of the Extreme Points on Photovoltaic Patterns using a new Asymptotic Perturbed Extremum Seeking Control scheme. *Energy Convers. Manag.* **2017**, *144*, 286–302.
43. Bizon, N.; Kurt, E. Performance Analysis of Tracking of the Global Extreme on Multimodal Patterns using the Asymptotic Perturbed Extremum Seeking Control Scheme. *Int. J. Hydrogen Energy* **2017**, *42*, 17645–17654.
44. Pukrushpan, J.T.; Stefanopoulou, A.G.; Peng, H. Control of fuel cell breathing. *IEEE Control. Syst. Mag.* **2004**, *24*, 30–46.
45. Kunusch, C.; Puleston, P.F.; Mayosky, M.A.; Riera, J. Sliding mode strategy for PEM fuel cells stacks breathing control using a super-twisting algorithm. *IEEE Trans. Control. Syst. Technol.* **2009**, *17*, 167–174.
46. Pukrushpan, J.T.; Stefanopoulou, A.G.; Peng, H. *Control of Fuel Cell Power Systems*; Springer: New York, NY, USA, 2004.
47. SimPowerSystems TM Reference, Hydro-Québec and the MathWorks, MathWorks Inc., Natick, MA 01760-2098, United States. 2010. Available online: http://www.hydroquebec.com/innovation/en/pdf/2010G080-04A-SPS.pdf (accessed on 29 October 2020).
48. Bizon, N. Energy Efficiency of Fuel Cell/Renewable Energy Sources Hybrid Power Source with Controlled Fuelling Flows. *Mathematics* **2020**, *8*, 151–173.
49. Bizon, N. Efficient fuel economy strategies for the Fuel Cell Hybrid Power Systems under variable renewable/load power profile. *Appl. Energy* **2019**, *251*, 113400–113518.

50. Bizon, N. Sensitivity analysis of the fuel economy strategy for a fuel cell hybrid power system using fuel optimization and load-following based on air control. *Energy Convers. Manag.* **2019**, *199*, 111946.
51. Restrepo, C.; Ramos-Paja, C.A.; Giral, R.; Calvente, J.; Romero, A. Fuel cell emulator for oxygen excess ratio estimation on power electronics applications. *Comput. Electr. Eng.* **2012**, *38*, 926–937.